NJC

ROYAL SOCIETY OF CHEMISTRY

PAPER

View Article Online
View Journal | View Issue

Cite this: *New J. Chem.*, 2025, **49**, 3987

Functionalized 1,3-dipyrrolyl-1,3-diketone difluoroboron complexes†

Ankitha M. Shenoy, Premie P. Fernandes and Vellanki Lakshmi *

Received 23rd October 2024,
Accepted 31st January 2025

DOI: 10.1039/d4nj04611k

rsc.li/njc

BF_2 complexes of 1,3-dipyrrolyl-1,3-diketones are highly emissive compounds and well known to be π-electronic anion-responsive systems because of their role in the formation of ion-pair assemblies. Despite their impressive electronic properties, their broader potential remains unexplored. Here, we synthesized a series of novel mono-functionalized π-electronic BF_2 complexes of 1,3-dipyrrolyl-1,3-diketones. Controlled functionalization was achieved by selectively introducing formyl, iodo, nitro and amine groups at the α-position of the unsubstituted pyrrole of 1,3-dipyrrolyl-1,3-diketone BF_2 complexes. Single crystal X-ray diffraction studies of compounds **2** and **4** provided definitive evidence of their molecular structures and confirmed selective functionalization. Detailed photophysical and electrochemical studies revealed the alteration of electronic properties through the choice of functional groups as evidenced by distinct absorption and emission profiles. Furthermore, DFT calculations complemented the experimental findings by providing insights into the bandgap energies and molecular stability of the compounds. These functionalized BF_2 complexes represent valuable building blocks for developing new derivatives with applications spanning organic electronics, bioimaging, and chemosensors.

Introduction

Stable organoboron complexes with remarkable adaptability have emerged as potential functional luminophores among fluorescent dyes.[1–5] The most commonly used boron dyes (Chart 1) include boron–dipyrromethene (BODIPY) complexes,[6–8] aza-based BODIPYs[9–11] and difluoroboron β-diketonate complexes (BF_2-bdks).[1,12,13] These dyes exhibit high absorption coefficients, significant Stokes shifts, high quantum yields (ϕ_f), and tunable absorption/emission profiles from visible to near-infrared (NIR region) in both solution and solid states.[1,14–18] They have been explored for potential applications in various areas, such as solar cells,[19–22] sensing,[11,23–25] bioimaging,[26–28] and photodynamic therapy.[29–33] Among the BF_2-bdks, 1,3-dipyrrolyl-1,3-propanedione boron (DPDB) complexes have emerged as promising anion-responsive π-electronic systems with unique optical and electronic properties.[24,34,35] DPDBs having long-alkyl chain compounds are recognized for their ability to form ion-pair assemblies in the presence of anions with suitable cations.[36–38] The DPDB complexes exhibit high absorption coefficients and high fluorescence quantum yields (ϕ_f).[39–41] Additionally, the nature of the substituent on the pyrrole rings plays a crucial role in determining the optical properties of DPDBs.[35,41–43] However, further research is needed to utilize these highly emissive systems for applications like optoelectronics, photovoltaics, and bio-applications, leaving ample room for developing new systems and tuning their properties. The DPDB scaffold has been a relatively unexplored area of research due to the lack of suitable monomer units. The introduction of functional groups on DPDBs allows the modulation of their electronic and optical properties for various applications. Maeda *et al.* introduced the nitro and iodo functional groups on diethyl-substituted pyrrole containing DPDBs and studied their anion-responsive properties.[44] Their group had developed aryl substituted DPDBs using iodo functionalized DPDB complexes to study their packing structures in the presence of anions.[45,46] Given the potential of these highly emissive compounds, there is a need to develop functionalized systems. The strategic functionalization of DPDBs offers a powerful tool to tailor their optical properties for specific applications ranging from optoelectronics to biological probes. In this report, selective mono-functionalization of DPDB (compound **1**) at the

Synthesis and Materials Laboratory, Department of Chemistry, National Institute of Technology, Surathkal, Karnataka, 575025, India.
E-mail: lakshmi.vellanki@nitk.edu.in

† Electronic supplementary information (ESI) available: Experimental procedures, NMR and mass spectra, details of X-ray single crystal diffraction, photophysical characterization spectra, CV, and DFT calculations. CCDC 2388456 and 2388457. For crystallographic data in CIF or other electronic format see DOI: https://doi.org/10.1039/d4nj04611k

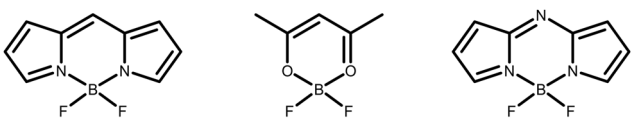

Chart 1 Common BF_2-complex dyes.

α-position was investigated to study its optical and electrochemical properties for understanding its electronic states.

Results and discussion

Synthesis and characterization

The investigation of the reactivity of molecular structure **1** indicates that the α-position of the 1,3-dipyrrolyl-1,3-propanedione BF_2-complex[47] (DPDB) is more reactive and susceptible for functionalization of the pyrrole ring. In our study, we focused on incorporating a range of common functional groups at this reactive centre to generate a variety of functionalized derivatives. Specifically, we explored the introduction of formyl, iodo, nitro, and amine groups at the α-position, each preferred for their diverse chemical properties and potential applications. Strategic functionalization allows fine-tuning of the DPDB's electronic and structural properties and provides possibilities for further synthetic modifications. With the systematic introduction of functional groups at the α-position, we aim to create a library of DPDB derivatives with tailored characteristics, potentially expanding their utility in fields such as materials science, catalysis, and molecular recognition.

Formylated DPDBs show significant reactivity for nucleophilic substitution reactions, making the –CHO group a key functional group for tuning and modifying the properties of synthesized compounds. Given this importance, we initiated our study with the formylation of compound **1**. The –CHO group was introduced onto the pyrrole carbon of DPDB using the Vilsmeier–Haack reaction by treating compound **1** with the Vilsmeier reagent, composed of excess equivalents of DMF and $POCl_3$ in 1,2-dichloroethane solvent. Initial attempts at formyl functionalization, involving direct addition of compound **1** to the Vilsmeier reagent (65 equiv. of DMF and 25 equiv. of $POCl_3$) and heating at 55 °C, led to the incomplete conversion of the starting materials. However, we optimized the condition by reversing the addition order. Adding Vilsmeier reagent to compound **1** at room temperature and further heating to 55 °C for 2 h resulted in the complete consumption of the starting materials (Scheme 1). The crude reaction mixture was purified by silica gel column chromatography, affording the formylated DPDB compound **2** as a yellow solid in 30% yield. Notably, despite our efforts, electrophilic substitution resulted only in mono-formyl DPDB. The insertion of one formyl group in the DPDB compound decreased its affinity towards additional electrophiles, making further functionalization of pyrrole challenging. This observation suggests that more vigorous conditions and a more detailed study may be necessary to introduce multiple formyl groups.

Halogenated DPDBs offer significant potential for developing novel DPDB-based systems, chiefly due to their reactivity in Pd-catalysed coupling reactions and nucleophilic substitution reactions. Using halogenated derivatives as synthetic intermediates, a wide range of functional groups can be introduced, allowing for the creation of complex and diverse molecular structures. To explore this potential, we attempted to synthesize both iodinated and brominated derivatives of compound **1**. The iodination reaction was successfully carried out by reacting compound **1** in tetrahydrofuran (THF) with 1.05 equivalents of *N*-iodosuccinimide (NIS) at −5 °C to −10 °C and then allowing to stir additionally for 1 h under the same conditions (Scheme 1). The selective iodination at the α-position of DPDB yielded a mono-iodinated DPDB derivative compound **3** as a yellow solid in 40% yield. Our iodination results are consistent with those reported by Maeda *et al.*, who also carried out an iodination reaction using NIS on a diethyl-substituted pyrrole-based BF_2 complex.[45] However, our attempts to obtain brominated derivatives using *N*-bromosuccinimide (NBS) and liquid bromine were unsuccessful, resulting in a complicated mixture of products. The successful synthesis and characterization of the mono-iodo DPDB derivative (compound **3**) demonstrate the potential for further functionalization of this complex. However, the challenges encountered in bromination highlight the need for alternative strategies or reaction conditions when introducing different halogen substituents.

The nitration of compound **1** was carried out using a mixture of concentrated acetic acid and nitric acid at 0 °C for

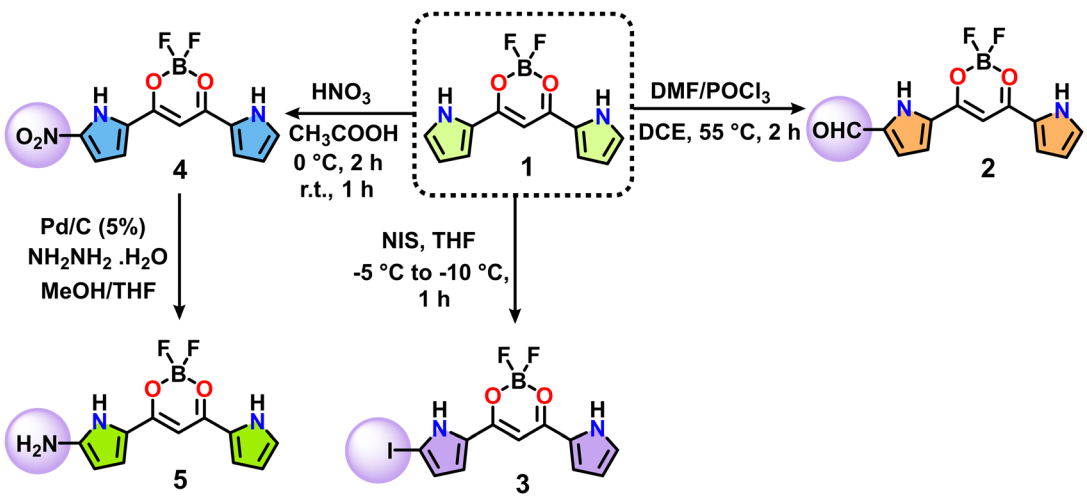

Scheme 1 Synthesis of mono-functionalized 1,3-dipyrroyl-1,3-diketone BF_2 complexes **2–5**.

2 h and for 1 h at room temperature (Scheme 1). Under these conditions, electrophilic substitution produced exclusively the mono-nitro derivative of compound **1**. Further purification of the crude product was achieved by silica gel column chromatography, yielding compound **4** as an orange solid in 41% yield. It is worth noting that Maeda *et al.* previously reported a similar nitration under similar conditions on a diethylsubstituted pyrrole-based BF_2 complex, which supports the viability of our approach.[44] Following the successful nitration of DPDB, the nitro compound was reduced to amine under Pd/C catalytic conditions using hydrazine hydrate as a reducing agent. The reaction mixture was refluxed for 1 h in a 1 : 1 ratio of methanol/tetrahydrofuran solvent (Scheme 1). Subsequent purification of a crude compound through silica gel chromatography yielded compound **5** as a red solid in 45% yield. It is worth noting that electron-withdrawing groups like –CHO and $–NO_2$ usually deactivate molecules and change their molecular orientation. This effect controls the introduction of multiple functional groups.

All the synthesized compounds **1–5** are freely soluble in common organic solvents such as dichloromethane (DCM), ethyl acetate (EtOAc), acetone, tetrahydrofuran (THF), chloroform ($CHCl_3$), dimethyl sulphoxide (DMSO), dimethyl formamide (DMF) and methanol (MeOH). Compounds **1–5** were characterized by ^{1}H, ^{13}C, ^{19}F, ^{11}B NMR, FT-IR, and MS spectroscopic techniques (Fig. S1–S26, ESI†). The ^{1}H NMR spectra of compound **1** exhibited three sets of signals for six protons of pyrrole carbons and two sets of signals for bridged –CH and –NH protons. Upon mono-functionalization, the DPDB complexes displayed distinct signals in the region of 5.5–14.0 ppm, corresponding to five pyrrole protons, two –NH protons, and one bridged –CH proton, due to their unsymmetrical nature. As shown in Fig. 1, distinct signals in ^{1}H NMR spectra at 9.74 ppm and 6.49 ppm corresponding to aldehyde (–CHO) and amine ($–NH_2$) groups, respectively, reveal their identity in compound **2** and compound **5**. The NH proton of the pyrrole ring in compound **4**, bearing a $–NO_2$ substituent, exhibited a downfield shift of 1.7 ppm compared to compound **1**, attributed to the electron-withdrawing nature of the nitro group. Conversely, the NH proton of the pyrrole ring in compound **5** bearing the amine substituent showed an up-field shift of 0.7 ppm due to the electron-donating nature of the amine group. The integration values obtained from these spectra further validated the structural composition of each compound. ^{19}F NMR of compounds **1–5** showed signals in the region of −138 to −141 ppm. Interestingly, compound **5** showed an up-field shift of 1.8 ppm in ^{19}F NMR, similar to ^{1}H NMR compared to **1** due to the electron-donating ability of the amine group. On the other hand, a singlet was observed in ^{11}B NMR spectra in the range of −0.18 to −0.36 ppm, respectively, for compounds **1–5** (Fig. 1). FT-IR spectroscopy (Fig. 2) provided additional insights, revealing the characteristic identities at 1668, 591, 1356, and 3383 cm^{-1} corresponding to –CHO in compound **2**, C–I in compound **3**, N–O for $–NO_2$ in compound **4**, and N–H for NH_2 in compound **5**, respectively. Furthermore, all compounds exhibit C=C stretching around 1562–1586 cm^{-1} and N–H stretching of pyrroles in the region of 3410–3492 cm^{-1}, consistent with the core DPDB structure. Molecular ion peaks in ESI-MS analysis provided definitive evidence confirming the molecular identities of the target compounds. All these spectroscopic findings precisely support the formation and molecular structures of compounds.

X-ray single crystal structures

Solid-state structures of compounds **2** and **4** were determined by single-crystal X-ray diffraction analysis, as shown in Fig. 3.

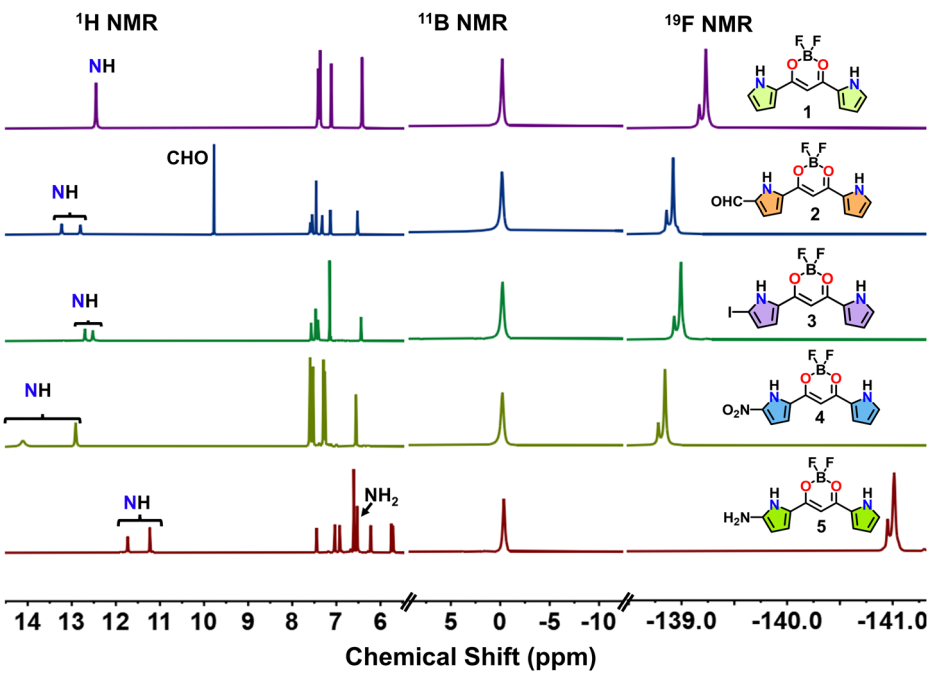

Fig. 1 ^{1}H, ^{11}B and ^{19}F NMR spectral changes of compounds **1–5** in DMSO-d_6.

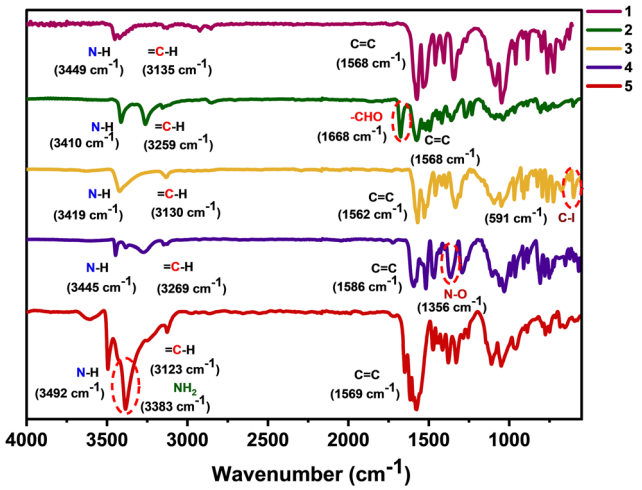

Fig. 2 FT-IR spectra of compounds **1–5**.

Single crystals of both compounds **2** and **4** were successfully obtained by the slow vapour diffusion of cyclohexane into an ethyl acetate solution at room temperature. The ORTEP plot of both compounds **2** and **4** at a 50% probability level is given in Fig. S27 (ESI†), and the parameters are tabulated in Table S1 (ESI†). Compound **2** bearing the –CHO group crystallized as orange plate-shaped crystals, revealing an orthorhombic system with a space group, $Pca2_1$, and a planar geometry. Fig. 3A–C illustrates the top and side views of the structure along with the packing diagram in a unit cell, where edge-to-end packing is observed. The crystal structure of compound **2** contains two molecules of compound **2** and three water molecules bound by intermolecular hydrogen bonding. The molecular structure features a formyl (–CHO) group located at the α-position of one of the appended pyrrole rings. Intermolecular hydrogen bonding is observed between the oxygen of the –CHO group and the NH of unsubstituted pyrrole, with N(–H)···O distances of 2.084 Å and 2.124 Å, as shown in Fig. 3C. The difference in bond distances is due to the layered antiparallel stacking of molecules caused by the intermolecular hydrogen bonding by the two water molecules. The hydrogen bonding network can be described as N1_1(–H)···O(–H2)···H–O–H···H(–N2_2) resulting from the hydrogen bonding interactions between the pyrrole NH and solvent molecules having hydrogen bond distances of 1.972 Å and 1.989 Å. The formyl-substituted pyrrole NH of one molecule binds with O–(H2), which then binds with the second water molecule. The second water molecule further forms a hydrogen bond with the formyl-substituted pyrrole NH.

The molecular structure of compound **4** is similar to that of compound **2**, exhibiting a planar geometry. Compound **4** existed as orange block-shaped crystals in a triclinic crystal system with a space group, $P\bar{1}$. Fig. 3D and E present the top and side views of compound **4**. The structure comprises one $–NO_2$ group at the α-position of one of the appended pyrrole rings. Compound **4** forms a dimeric structure with an interplanar distance of 3.134 Å between the anti-parallel face-to-face

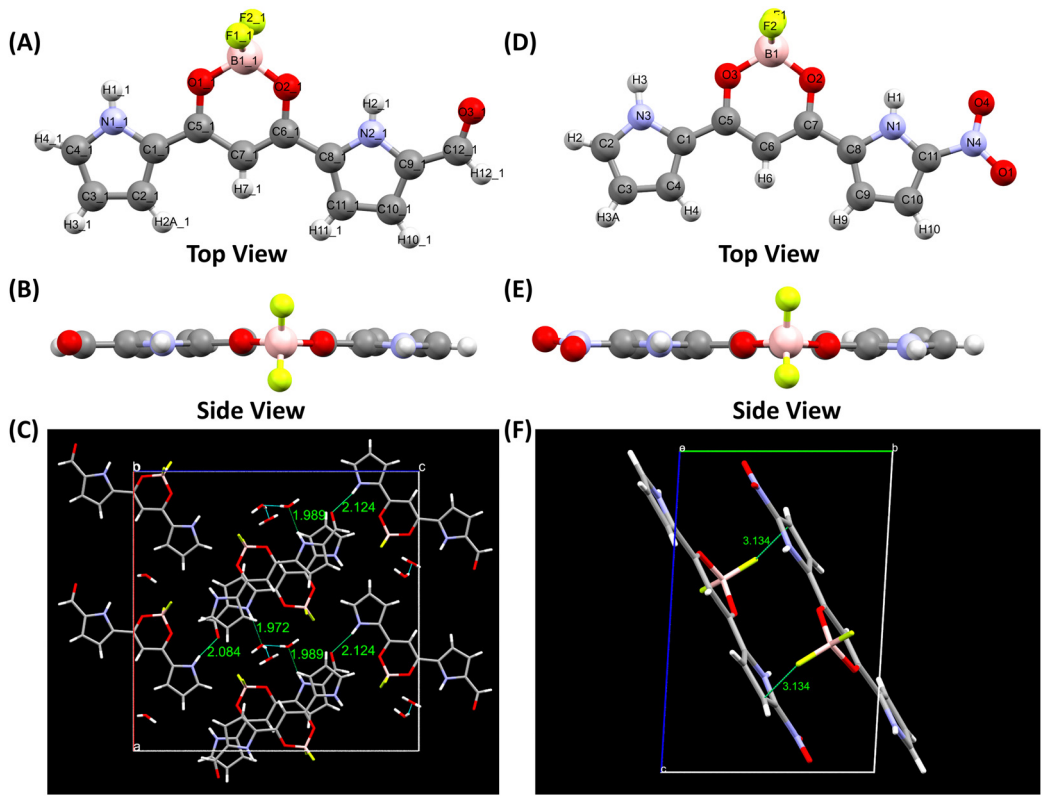

Fig. 3 (A) Front view and (B) top view of compound **2** structure. (C) Packing diagram of compound **2** in a unit cell. (D) Front view and (E) top view of compound **4** structure. (F) Packing diagram of compound **4** in a unit cell.

π–π stacking interactions, as shown in Fig. 3F. The intermolecular hydrogen bonding interactions observed in the crystal structure are given in Table S2 (ESI†). Fig. 3F displays the packing arrangement of molecules with two molecules per unit cell. From a polyhedral view, the bond angles of F1–B1–F2, F1–B1–O2, F2–B1–O3 and O3–B1–O2 were found to be 110.12°, 108.91°, 108.93° and 112.68°, respectively.

Theoretical calculations

Density functional theory (DFT) calculations for all compounds were performed using the Gaussian 09W program to demonstrate the effect of the functional group on the optical properties and electronic distribution of compounds **2–5** with respect to the parent compound **1**. These calculations were performed at the level of B3-LYP/6-31G(d,p)[48] for compounds containing C, H, B, N, O, and F and using the LANL2DZ basis set for I atoms. The optimized geometries are presented in Fig. S28 (ESI†). Table S3 (ESI†) shows the cartesian coordinates of all compounds with their stabilization energies. The excited state energy calculations were performed using the TDA method and the B3-LYP/6-31G+(d,p) basis set for C, H, B, N, O, and F and the LANL2DZ basis set for I in CH_2Cl_2 and the molecular contributions of HOMOs and LUMOs for $S_0 \rightarrow S_1$ transition are summed up in Table S4 (ESI†). The electron density surface plots mapped with electrostatic potentials (ESP) for compounds **1–5** are given in Fig. 4. From the ESP plot, it is observed that compounds **1**, **2** and **4** show a higher electron density on the BF_2 complexed region and over the functional groups, while the electron density on the aromatic conjugated region is less owing to the electron-withdrawing substituents *viz.* –CHO and $–NO_2$. Similarly, in compound **3** it's evident that the electron density is spread equally across the structure of the molecule due to the less electronegative iodine substituent. In compound **5**, the electron density is the highest on the BF_2 complexed region amongst all other derivatives, with the aromatic pyrrole rings also having sufficiently good electron density because of the electron-donating $–NH_2$ group. The molecular orbital plot shows that unlike compound **1**, which is symmetric, the highest occupied molecular orbitals (HOMOs) and lowest unoccupied molecular orbitals (LUMOs) of compounds **2** and **3** were distributed over the π-electronic core along with formyl and iodo functional groups. However, the delocalization over the iodo group in the LUMO of **3** is not observed due to the less electronegative and weaker π-acceptor nature of iodine (Fig. 5). For compounds **4** and **5**, the HOMO was delocalized over the main π-electronic core. Additionally, the –C–O/–C═O group located in the unsubstituted pyrrole in compound **4** and in the amine-substituted pyrrole in compound **5** was not involved in the delocalization. However, the LUMO was more distributed in the nitro-substituted pyrrole for **4** and in the unsubstituted pyrrole for compound **5**. These observations supported the ICT for compounds **4** and **5** in more polar solvents.[44] The electron-withdrawing groups like –CHO and $–NO_2$ pull the electron density of the bonding molecular orbitals out of the substituted pyrrole ring and the six-membered BF_2 complex, as seen in HOMO delocalization plots of compounds **2** and **4**. The band gap was calculated as 3.32–3.37 eV, which was significantly lowered upon functionalization at the α-position of the pyrrole group compared to that of parent compound **1** (3.63 eV). The LUMO of compound **4**, having $–NO_2$, was found to have the least energy of 3.137 eV, thereby indicating that the nitro group significantly stabilized the excited state by lowering its HOMO and LUMO levels, whereas the electron-donating substituent, the amine group in compound **5**, destabilized the frontier molecular orbitals.

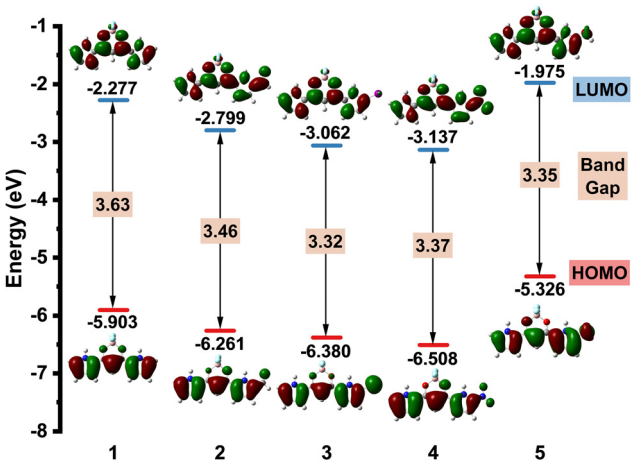

Fig. 5 Molecular energy diagram with HOMOs, LUMOs and energy band gaps of compounds **1–5**.

Photophysical properties

The absorption properties of compounds **1–5** were studied in dichloromethane (CH_2Cl_2) solvent, and the representative data and graph are presented in Table 1 and Fig. 6A, respectively. The parent compound **1** exhibited λ_{abs} at 432 nm in its UV-visible absorption spectrum.[47] The mono-functionalized DPDBs **2–5** showed a strong absorption band between 437 and 477 nm, corresponding to the π–π* electronic transition, with a shoulder peak on the higher energy side in the range of 425–460 nm. The introduction of functional groups at the α-position of the parent compound resulted in bathochromic shifts of 5–45 nm

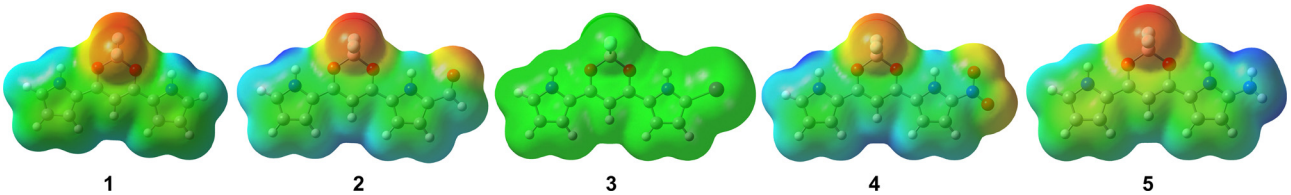

Fig. 4 Electron density surface plots mapped with electrostatic potential of compounds **1–5**.

compared to compound **1**, depending on the functional group. The maximum bathochromic shift of 45 nm was observed for compound **5**, having the amine substituent due to the electron-donating nature of the amine group. The lone pair of electrons in the donating group extends the π-conjugation and stabilizes the molecular orbital system. Among compounds **1–5**, compound **4** ($-NO_2$) and compound **5** ($-NH_2$) displayed broad absorption spectra, which can be attributed to the contribution of a wide range of energy levels with extended conjugation, and structural flexibility, which enhances the intramolecular charge transfer (ICT) behaviour compared to other compounds.[44,49]

Steady-state fluorescence properties of compounds **1–5** were studied in CH_2Cl_2 solvent, excited at λ_{max} of absorbance to obtain further insights into their electronic properties. All the compounds exhibited a peak maximum in the range of 451–504 nm, as shown in Fig. 6B. A bathochromic shift of 6–53 nm was observed compared to the parent compound **1**. Compounds **4** and **5** displayed the highest peak maxima at 502 and 504 nm with a broader emission band likely resulting from ICT transitions. The fluorescence quantum yield (ϕ_f) of compounds **2–5** varied in the range of 0.2–60%, as shown in Table 1, depending on the substituent.

The lifetimes of compounds **1–5** were measured using the time-correlated single photon counting (TCSPC) technique, and the decays fitted to single exponential are presented in Fig. 7 and Table 1. The singlet lifetimes of compounds **1–5** are in line with the quantum yields. Compound **1** with quantitative quantum yield showed a lifetime of 2.23 ns with a single exponential fit. Furthermore, compounds **2** and **3** with formyl and iodo groups with high quantum yields (ϕ_f) of 52% and 60% showed lifetimes of 1.21 ns and 1.41 ns, respectively. However, compounds **4** and **5** with nitro and amino functional groups with lower quantum yields (ϕ_f) of 16% and 0.2% showed lifetimes with bi-exponential fit in the range of 0.67–4.26 ns, as presented in Fig. S29 (ESI†). Furthermore, the low quantum yields and poor lifetime results of compounds **4** and **5** can be attributed to the ICT of nitro and amine groups in DPDB complexes, which supports the poor steady-state emission properties of compounds **4** and **5** compared to compounds **1–3**. Additionally, the effect of the solvent on the lifetime of compound **2** was investigated in various solvents, revealing that the fluorescence decay was faster with increasing solvent polarity, as shown in Fig. S30 and Table S5 (ESI†).

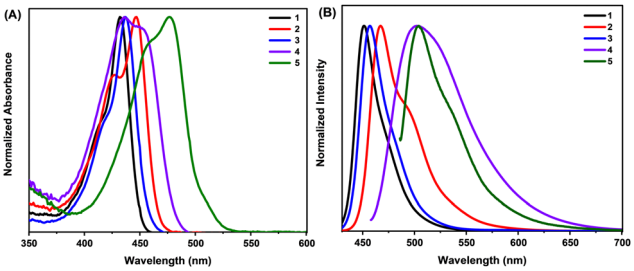

Fig. 6 (A) Normalized absorption and (B) normalized emission of compounds **1–5** in CH_2Cl_2 (5×10^{-6} M).

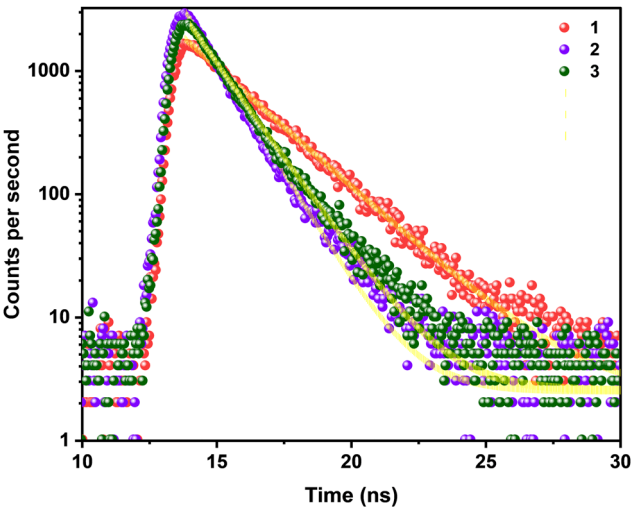

Fig. 7 Time-resolved fluorescence decay profiles of compounds **1–3** in CH_2Cl_2 solvent.

Solvatochromism

We performed solvent-dependent studies to understand the ground and excited state photophysical properties of compounds **1–5** through absorption and emission measurements in solvents by varying the polarities. Solutions of compounds **1–5** with a concentration of 5 μM in different solvents, including dichloromethane (DCM), tetrahydrofuran (THF), ethyl acetate (EtOAc), acetonitrile (ACN), dimethylformamide (DMF) and dimethyl sulfoxide (DMSO), were prepared and data are presented in Table S6 (ESI†). The absorption and emission spectra of all the compounds displayed only minor changes with increasing polarity of aprotic solvents from DCM to ACN. However, a bathochromic shift of ~40 nm in the absorbance and ~15 nm in emission ($\lambda_{ex} = \lambda_{max}$) was observed in polar aprotic solvents such as DMF and DMSO for compounds **1–5**. The redshift can be attributed to the formation

Table 1 Photophysical and electrochemical properties of compounds **1–5**

Compounds	λ_{abs} [a] (nm)/ε ($\times 10^4$)	λ_{em} (nm)	ϕ_f [a]	τ (ns)	χ^2	λ_{abs} [b] (nm)	λ_{em} [b] (nm)	ϕ_f [b] (%)	E_{red} [c] (V)	E_{ox} [c] (V)
1	432 (7.79)	451	Quantitative	2.23	1.098	314, 478	527	5.6	−1.66	0.72
2	427 (6.68), 447 (4.88)	467	52%	1.21	1.231	369, 487	555	7.4	−1.79, −2.14	0.90
3	437 (8.65)	457	60%	1.41	1.171	476, 575	619	1.4	−1.26	0.81
4	436 (3.36), 452 (3.19)	502	16%	0.67, 3.28	1.221	—	—	—	−0.73, −1.24	1.05
5	456 (3.97), 477 (4.61)	504	0.2%	1.34, 4.26	1.129	—	—	—	−1.90	0.10, 0.36

[a] Measured in CH_2Cl_2 (5×10^{-6} M). [b] Measured in a solid state. [c] E_{ox} is the onset oxidation potential and E_{red} is the reduction potential measured in acetonitrile (V *vs.* Fc/Fc^+).

of strong hydrogen bond interactions between the solvent and solute molecules, which stabilize the excited states (Fig. 8) (Fig. S33, ESI†). The photostability of compounds **2–5** was studied in acetonitrile solvent under continuous UV irradiation (319 nm) for 3 h. The optical density at λ_{max} remained relatively constant for all compounds, demonstrating their excellent photostability (Fig. S31 and S32, ESI†).

Solid-state properties

Broader absorption and emission bands were observed for compounds **1–3** in the solid state compared to the solution state likely due to the strong intermolecular interactions, as shown in Fig. 9 and Table 1. Compound **1** showed absorption maxima at 478 nm with a shoulder at 314 nm, while compounds **2** and **3** displayed maxima at 487 and 476 nm with shoulders at 369 and 575 nm, respectively. When exposed to UV radiation at 365 nm, compounds **1–3** exhibited distinct fluorescence of yellow for **1**, bright yellow for **2**, and red for **3**. In contrast, compounds **4** and **5** did not fluoresce under the UV light. The fluorescence emission spectra of compounds **1–3** exhibited emission peaks at 527, 555, and 619 nm, respectively, obtained by exciting at their corresponding absorption maxima (λ_{max}). The incorporation of the electron-withdrawing group, –CHO, into compound **1** results in improved solid-state emission, with a quantum yield (ϕ_f) of 7.4% compared to 5.6% of compound **1**. However, compound **3** exhibited a significantly large bathochromic shift of 92 nm with a reduced quantum yield (ϕ_f) of 1.4%. This pronounced redshift in the solid state can be attributed to the intermolecular interaction between the polar electron-withdrawing substituents in the adjacent molecules stabilizing the excited state and lowering the band gap between the excited and ground states.[50] Moreover, according to exciton coupling theory, the formation of J-aggregates, as seen in Fig. 3 (head-to-tail alignment of molecules), contributes to the observed redshift.[51]

Electrochemical properties

Electrochemical studies were performed using cyclic voltammetry (CV) for all compounds **1–5** in deoxygenated acetonitrile using 0.1 M tetrabutylammonium perchlorate (TBAP) as a supporting electrolyte at room temperature and ferrocene as the external standard. All compounds **1–5** exhibited one or two irreversible oxidation peaks and reversible/irreversible reduction peaks. Interestingly, compound **2** with the –CHO

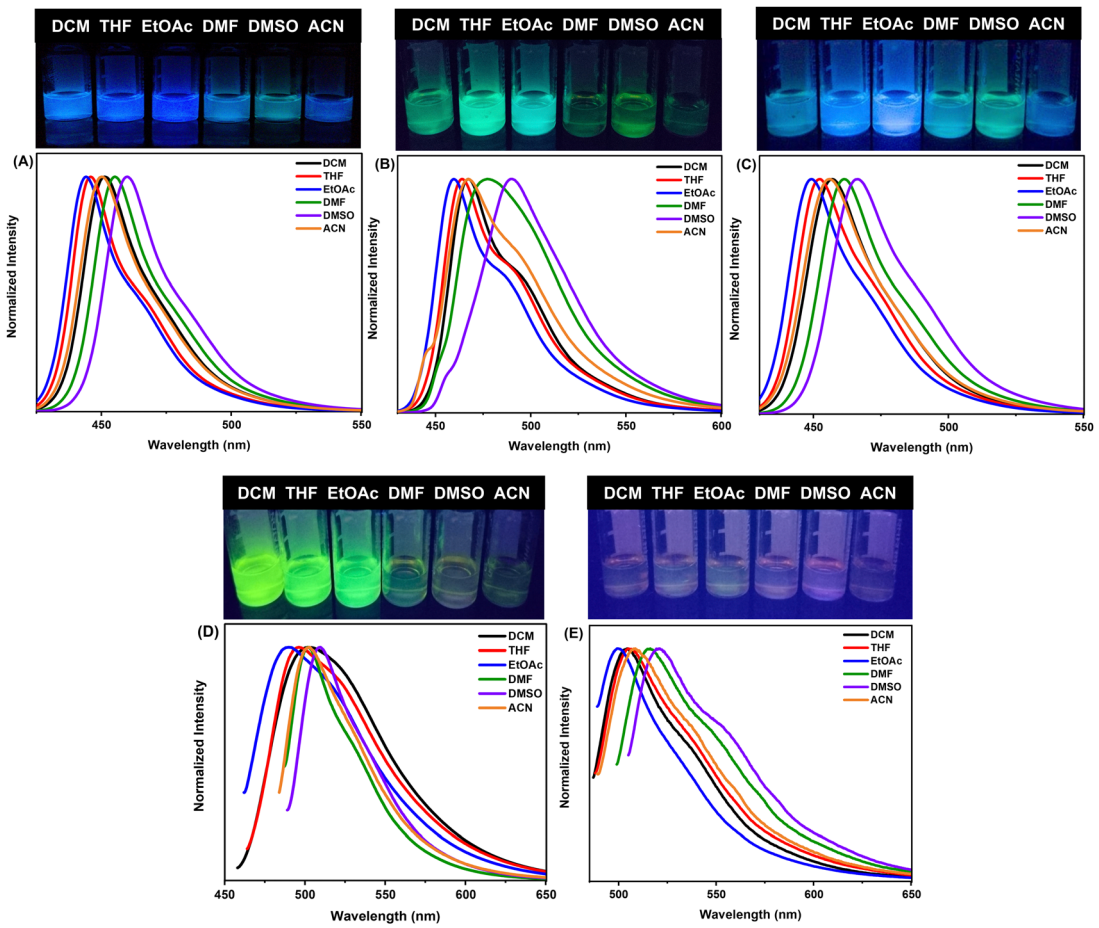

Fig. 8 Normalized emission spectra of compounds (A) **1**, (B) **2**, (C) **3**, (D) **4**, and (E) **5** in various solvents ($\lambda_{ex} = \lambda_{max}$).

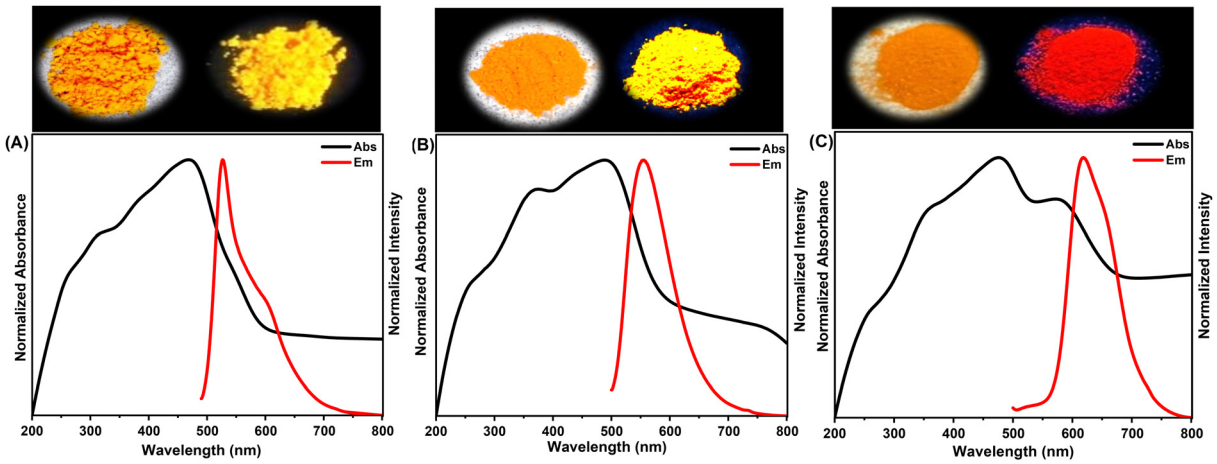

Fig. 9 Normalized solid-state absorption (black) and emission (red) spectra of compounds (A) **1**, (B) **2**, and (C) **3** ($\lambda_{ex} = \lambda_{max}$). Digital images taken under a UV lamp at 365 nm (right) and day light (left) are shown above the spectra.

substituent, having the capability to be oxidized and reduced, exhibited two reversible reduction peaks at −1.79 V and −2.14 V and one irreversible oxidation wave with the onset at 0.90 V (Table 1 and Fig. S34, ESI†), indicating the difficulty in both oxidation and reduction compared to **1**. Compounds **3** and **4**, having –I and $-NO_2$ substituents at the α-position of the pyrrole ring of DPDB, showed an anodic shift in reduction potentials compared to the parent compound **1**, indicating that compounds **3** and **4** are easier to reduce. Conversely, compound **5** with the electron-donating substituent $-NH_2$ showed a cathodic shift in the reduction potential compared to **1**. Among compounds **1–5**, compound **5** with the amine group showed two oxidation waves with the onset at 0.10 V and 0.36 V, whereas compounds **1–4** showed oxidation potentials ranging from 0.72 to 1.05 V, indicating that compound **5** is easier to oxidize (Fig. 10). The difficulty in reduction and ease of oxidation with an electron-rich amine functional group can be attributed to the effective conjugation of amine with the DPDB structure. These redox properties suggest that the type of functional group alters the electronic properties of DPDB compounds.

Conclusions

In conclusion, we have synthesized mono-functionalized 1,3-dipyrrolyl-1,3-diketone BF_2 complexes, each containing formyl, iodo, nitro, and amino as a functional group at the α-position of unsubstituted pyrrole. Spectroscopic and single crystal structure analyses confirmed the identity of molecular structures. These functional groups significantly altered the photophysical and electrochemical properties, resulting in a bathochromic shift compared to parent compound **1** due to the increased π-electronic conjugation. A solvent study of absorption and

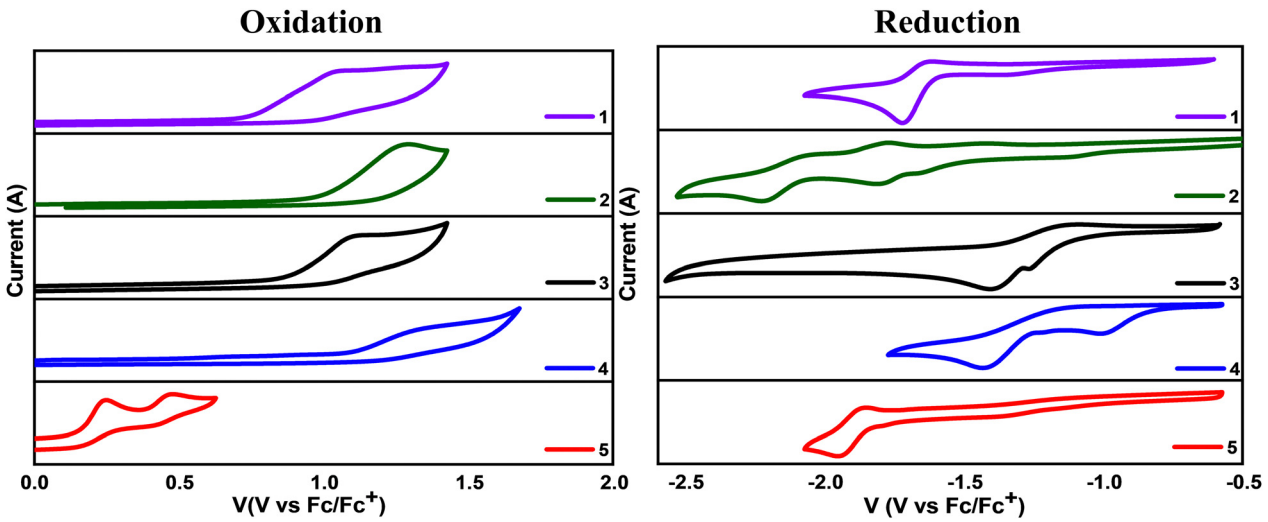

Fig. 10 Electrochemical redox data of compounds **1–5** in acetonitrile containing 0.1 M tetrabutylammonium perchlorate as a supporting electrolyte recorded at scan rates of 100 mV sec^{-1} (**1** and **2**) and 50 mV sec^{-1} (**3**, **4** and **5**).

emission was performed using a range of polar aprotic solvents, to understand the solvent effects. Interestingly, high quantum yields and good lifetimes in solution state were exhibited by compounds **1–3** along with high solid-state emission, whereas compounds **4** and **5** showed poor properties due to the intramolecular charge transfer behavior from $-NO_2$ and $-NH_2$ groups. These findings open new possibilities for tailoring the properties of BF_2 complexes. Selective functionalization makes them promising candidates as primary building blocks for developing DPDB derivatives and provides valuable insights for future research on various applications in organic electronics, bioimaging, sensing, *etc.*

Data availability

The data supporting this article have been included as part of the ESI,† including spectral data. The crystallographic data for **2** and **4** have been deposited at the CCDC under 2388456 and 2388457.†

Conflicts of interest

There are no conflicts to declare.

Acknowledgements

V. L. acknowledges the Science and Engineering Research Board (SERB), India, for partially supporting through the SRG (2021/002251) grant. A. M. S. and P. P. F. thank UGC for providing the SJSGC fellowship and NITK for a research fellowship, respectively. The authors gratefully acknowledge the Department of Chemistry NITK, CRF-NITK, SCIF-IIT Dharwad and Single crystal XRD lab-VIT Vellore.

References

1 P.-Z. Chen, L.-Y. Niu, Y.-Z. Chen and Q.-Z. Yang, Difluoroboron β-diketonate dyes: Spectroscopic properties and applications, *Coord. Chem. Rev.*, 2017, **350**, 196–216.
2 D. Frath, J. Massue, G. Ulrich and R. Ziessel, Luminescent Materials: Locking π-Conjugated and Heterocyclic Ligands with Boron(III), *Angew. Chem., Int. Ed.*, 2014, **53**, 2290–2310.
3 A. Loudet and K. Burgess, BODIPY Dyes and Their Derivatives: Syntheses and Spectroscopic Properties, *Chem. Rev.*, 2007, **107**, 4891–4932.
4 A. N. Bismillah and I. Aprahamian, Fundamental studies to emerging applications of pyrrole-BF_2 (BOPHY) fluorophores, *Chem. Soc. Rev.*, 2021, **50**, 5631–5649.
5 A. C. Murali, P. Nayak and K. Venkatasubbaiah, Recent advances in the synthesis of luminescent tetra-coordinated boron compounds, *Dalton Trans.*, 2022, **51**, 5751–5771.
6 V. Lakshmi, M. Rajeswara Rao and M. Ravikanth, Halogenated boron-dipyrromethenes: synthesis, properties and applications, *Org. Biomol. Chem.*, 2015, **13**, 2501–2517.
7 N. A. Bumagina, E. V. Antina, A. A. Ksenofontov, L. A. Antina, A. A. Kalyagin and M. B. Berezin, Basic structural modifications for improving the practical properties of BODIPY, *Coord. Chem. Rev.*, 2022, **469**, 214684.
8 C. S. Mahanta, V. Ravichandiran and S. P. Swain, Recent Developments in the Design of New Water-Soluble Boron Dipyrromethenes and Their Applications: An Updated Review, *ACS Appl. Bio Mater.*, 2023, **6**, 2995–3018.
9 Z. Shi, X. Han, W. Hu, H. Bai, B. Peng, L. Ji, Q. Fan, L. Li and W. Huang, Bioapplications of small molecule Aza-BODIPY: from rational structural design to *in vivo* investigations, *Chem. Soc. Rev.*, 2020, **49**, 7533–7567.
10 P. Rana, N. Singh, P. Majumdar and S. Prakash Singh, Evolution of BODIPY/aza-BODIPY dyes for organic photoredox/energy transfer catalysis, *Coord. Chem. Rev.*, 2022, **470**, 214698.
11 M. Kaur, A. Janaagal, N. Balsukuri and I. Gupta, Evolution of Aza-BODIPY dyes-A hot topic, *Coord. Chem. Rev.*, 2024, **498**, 215428.
12 E. B. A. Paez, S. Curcio, N. P. Neme, M. J. S. Matos, R. S. Correa, F. J. Pereira, F. F. Hilário, T. Cazati and J. G. Taylor, Synthesis, photophysical and electrochemical properties of novel and highly fluorescent difluoroboron flavanone beta-diketonate complexes, *New J. Chem.*, 2020, **44**, 14615–14631.
13 X.-G. Yang, P.-P. Yin, Q. Wang, S.-Y. Yang, Y. Li, X. Gao, J. Song, X.-Y. Zhang and Z. Li, Aggregation-Induced Emission of Curcuminoid-BF_2 Complex for Phosphor-Converted Red Light-Emitting Diode, *Inorg. Chem.*, 2024, **63**, 17346–17350.
14 J. Wang, N. Boens, L. Jiao and E. Hao, Aromatic [*b*]-fused BODIPY dyes as promising near-infrared dyes, *Org. Biomol. Chem.*, 2020, **18**, 4135–4156.
15 H. A. A. El-Ali, J. Jing and X. Zhang, Solid-state emissive O-BODIPY dyes with bimodal emissions across red and near infrared region, *RSC Adv.*, 2019, **9**, 16246–16251.
16 J. Wang, C. Yu, E. Hao and L. Jiao, Conformationally restricted and ring-fused aza-BODIPYs as promising near infrared absorbing and emitting dyes, *Coord. Chem. Rev.*, 2022, **470**, 214709.
17 S. Shimizu, aza-BODIPY synthesis towards vis/NIR functional chromophores based on a Schiff base forming reaction protocol using lactams and heteroaromatic amines, *Chem. Commun.*, 2019, **55**, 8722–8743.
18 Y. Qi, W. Liu, T. Du, J. Wang and S. Jiao, Red/near-infrared (NIR) difluoroboron β-diketonate derivatives with reversible mechanochromism for cellular imaging, *Spectrochim. Acta, Part A*, 2025, **325**, 124986.
19 J. Min, T. Ameri, R. Gresser, M. Lorenz-Rothe, D. Baran, A. Troeger, V. Sgobba, K. Leo, M. Riede, D. M. Guldi and C. J. Brabec, Two Similar Near-Infrared (IR) Absorbing Benzannulated Aza-BODIPY Dyes as Near-IR Sensitizers for Ternary Solar Cells, *ACS Appl. Mater. Interfaces*, 2013, **5**, 5609–5616.
20 V. K. Shukla, G. Chakraborty, A. K. Ray and S. Nagaiyan, Red and NIR emitting ring-fused BODIPY/aza-BODIPY dyes, *Dyes Pigm.*, 2023, **215**, 111245.

21 R. Feng, T. Mori, T. Yasuda, H. Furuta and S. Shimizu, Panchromatic small-molecule organic solar cells based on a pyrrolopyrrole aza-BODIPY with a small energy loss, *Dyes Pigm.*, 2023, **210**, 111020.
22 Y. Mizuno, Y. Yisilamu, T. Yamaguchi, M. Tomura, T. Funaki, H. Sugihara and K. Ono, (Dibenzoylmethanato)-boron Difluoride Derivatives Containing Triphenylamine Moieties: A New Type of Electron-Donor/π-Acceptor System for Dye-Sensitized Solar Cells, *Chem. – Eur. J.*, 2014, **20**, 13286–13295.
23 P. Kaur and K. Singh, Recent advances in the application of BODIPY in bioimaging and chemosensing, *J. Mater. Chem. C*, 2019, **7**, 11361–11405.
24 Y. Haketa, K. Kamada and H. Maeda, Anion-Responsive Molecules That Exhibit Switching Two-Photon Optical Properties, *ChemPlusChem*, 2020, **85**, 1719–1729.
25 H. Li, P. Zhang, L. P. Smaga, R. A. Hoffman and J. Chan, Photoacoustic Probes for Ratiometric Imaging of Copper(II), *J. Am. Chem. Soc.*, 2015, **137**, 15628–15631.
26 L. Wang, Z. Xiong, X. Ran, H. Tang and D. Cao, Recent advances of NIR dyes of pyrrolopyrrole cyanine and pyrrolopyrrole *aza*-BODIPY: Synthesis and application, *Dyes Pigm.*, 2022, **198**, 110040.
27 Y. Ni and J. Wu, Far-red and near infrared BODIPY dyes: synthesis and application for fluorescent pH probes and bio-imaging, *Org. Biomol. Chem.*, 2014, **12**, 3774.
28 M. Collot, Recent advances in dioxaborine-based fluorescent materials for bioimaging applications, *Mater. Horiz.*, 2021, **8**, 501–514.
29 S. Wang, L. Gai, Y. Chen, X. Ji, H. Lu and Z. Guo, Mitochondria-targeted BODIPY dyes for small molecule recognition, bio-imaging and photodynamic therapy, *Chem. Soc. Rev.*, 2024, **53**, 3976–4019.
30 C. Liu, C. Liu, X. Ji, W. Zhao and X. Dong, Synthesis and Photodynamic Activities of Pyridine- or Pyridinium-Substituted Aza-BODIPY Photosensitizers, *J. Med. Chem.*, 2024, **67**, 15908–15924.
31 S. Mishra, D. Dos Santos, S. B. Shelar, K. Reess, A. Rück, P. A. Hassan, K. C. Barick and N. Agarwal, Photocytotoxic and cellular metabolism studies of curcuminoid-BF_2 nanoaggregates in human carcinoma cells, *J. Photochem. Photobiol., A*, 2024, **457**, 115902.
32 P. Chinna Ayya Swamy, G. Sivaraman, R. N. Priyanka, S. O. Raja, K. Ponnuvel, J. Shanmugpriya and A. Gulyani, Near Infrared (NIR) absorbing dyes as promising photosensitizer for photo dynamic therapy, *Coord. Chem. Rev.*, 2020, **411**, 213233.
33 I. Singh Yadav and R. Misra, Design, synthesis and functionalization of BODIPY dyes: applications in dye-sensitized solar cells (DSSCs) and photodynamic therapy (PDT), *J. Mater. Chem. C*, 2023, **11**, 8688–8723.
34 H. Maeda, Y. Haketa, T. Murata, E. Ohta, T. Murata and N. Yasuda, Self-assemblies of anionic-unit-introduced anion-responsive π-electronic molecules, *Org. Biomol. Chem.*, 2021, **19**, 7369–7373.
35 S. Kaname, Y. Haketa, N. Yasuda and H. Maeda, Cyclic Anion-Responsive π-Electronic Molecules That Overcome Energy Losses Induced by Conformation Changes, *Org. Lett.*, 2018, **20**, 3268–3272.
36 Y. Haketa, D. Katayama, S. Fukunaga, Y. Bando, T. Sakurai, W. Matsuda, S. Seki and H. Maeda, Ion-Free and Ion-Pairing Assemblies of Anion-Responsive π-Electronic Systems Possessing Directly Linked Alkyl Chains, *Chem. – Asian J.*, 2016, **11**, 2025–2029.
37 Y. Haketa, K. Urakawa and H. Maeda, First decade of π-electronic ion-pairing assemblies, *Mol. Syst. Des. Eng.*, 2020, **5**, 757–771.
38 Y. Haketa and H. Maeda, Dimension-controlled ion-pairing assemblies based on π-electronic charged species, *Chem. Commun.*, 2017, **53**, 2894–2909.
39 R. Sato, H. Okajima, S. Sugiura, Y. Haketa, Y. Kinoshita, H. Tamiaki, A. Sakamoto, H. Maeda and Y. Kobayashi, Excited-state dynamics of dipyrrolyldiketone difluoroboron complexes, *Phys. Chem. Chem. Phys.*, 2022, **24**, 1685–1691.
40 H. Maeda, M. Takayama, K. Kobayashi and H. Shinmori, Modification at a boron unit: tuning electronic and optical properties of π-conjugated acyclic anion receptors, *Org. Biomol. Chem.*, 2010, **8**, 4308–4315.
41 S. Sugiura, Y. Kobayashi, N. Yasuda and H. Maeda, Multiply aryl-substituted dipyrrolyldiketone boron complexes exhibiting anion-responsive emissive properties, *Chem. Commun.*, 2019, **55**, 8242–8245.
42 H. Maeda, T. Nishimura, Y. Haketa, H. Tanaka, M. Fujita and N. Yasuda, Ion-pairing assemblies of anion-responsive π-electronic systems bearing triazole moieties introduced by click chemistry, *J. Org. Chem.*, 2022, **87**, 7818–7825.
43 S. Sugiura, W. Matsuda, W. Zhang, S. Seki, N. Yasuda and H. Maeda, Ion-Pairing Assemblies Comprising Anion Complexes of π-Extended Anion-Responsive Molecules, *J. Org. Chem.*, 2019, **84**, 8886–8898.
44 A. Kuno and H. Maeda, Nitro-Substituted Dipyrrolyldiketone BF_2 Complexes as Electronic-State-Adjustable Anion-Responsive π-Electronic Systems, *Molecules*, 2021, **26**, 595.
45 H. Maeda and Y. Haketa, Selective iodinated dipyrrolyldiketone BF_2 complexes as potential building units for oligomeric systems, *Org. Biomol. Chem.*, 2008, **6**, 3091.
46 V. Lakshmi, Y. Haketa, R. Yamakado, N. Yasuda and H. Maeda, Dimension-controlled assemblies of anion-responsive π-electronic systems bearing aryl substituents with fan-shaped geometries, *Chem. Commun.*, 2017, **53**, 3834–3837.
47 H. Maeda and Y. Kusunose, Dipyrrolyldiketone Difluoroboron Complexes: Novel Anion Sensors With C–H···X^- Interactions, *Chem. – Eur. J.*, 2005, **11**, 5661–5666.
48 A. D. Becke, Density-functional thermochemistry. III. The role of exact exchange, *J. Chem. Phys.*, 1993, **98**, 5648–5652.
49 I. Esnal, J. Bañuelos, I. López Arbeloa, A. Costela, I. Garcia-Moreno, M. Garzón, A. R. Agarrabeitia and M. José Ortiz, Nitro and amino BODIPYS: crucial substituents to modulate their photonic behavior, *RSC Adv.*, 2013, **3**, 1547–1556.
50 R. M. Adhikari, D. C. Neckers and B. K. Shah, Photophysical Study of Blue, Green, and Orange-Red Light-Emitting Carbazoles, *J. Org. Chem.*, 2009, **74**, 3341–3349.
51 M. K. Bera, P. Pal and S. Malik, Solid-state emissive organic chromophores: design, strategy and building blocks, *J. Mater. Chem. C*, 2020, **8**, 788–802.

